Aerosol Science and Technology

ISSN: 0278-6826 (Print) 1521-7388 (Online) Journal homepage: http://www.tandfonline.com/loi/uast20

Aerosolization System for Experimental Inhalation Studies of Carbon-Based Nanomaterials

Amy K. Madl , Stephen V. Teague , Yongquan Qu , Daniel Masiel , James E. Evans , Ting Guo & Kent E. Pinkerton

To cite this article: Amy K. Madl , Stephen V. Teague , Yongquan Qu , Daniel Masiel , James E. Evans , Ting Guo & Kent E. Pinkerton (2012) Aerosolization System for Experimental Inhalation Studies of Carbon-Based Nanomaterials, Aerosol Science and Technology, 46:1, 94-107, DOI: 10.1080/02786826.2011.605813

To link to this article: http://dx.doi.org/10.1080/02786826.2011.605813

Published online: 28 Sep 2011.

Submit your article to this journal

Article views: 546

View related articles

Citing articles: 3 View citing articles

Full Terms & Conditions of access and use can be found at
http://www.tandfonline.com/action/journalInformation?journalCode=uast20

Download by: [University of North Texas] **Date:** 06 January 2017, At: 00:24

Aerosol Science and Technology, 46:94–107, 2012
Copyright © American Association for Aerosol Research
ISSN: 0278-6826 print / 1521-7388 online
DOI: 10.1080/02786826.2011.605813

Aerosolization System for Experimental Inhalation Studies of Carbon-Based Nanomaterials

Amy K. Madl,[1] Stephen V. Teague,[2] Yongquan Qu,[3] Daniel Masiel,[3] James E. Evans,[4] Ting Guo,[3] and Kent E. Pinkerton[1]

[1]*Center for Health and the Environment, University of California, Davis, California, USA*
[2]*Teague Enterprises, Woodland, California, USA*
[3]*Department of Chemistry, University of California, Davis, California, USA*
[4]*Department of Molecular and Cellular Biology, University of California, Davis, California, USA*

Assessing the human health risks associated with engineered nanomaterials is challenging because of the wide range of plausible exposure scenarios. While exposure to nanomaterials may occur through a number of pathways, inhalation is likely one of the most significant potential routes of exposure in industrial settings. An aerosolization system was developed to administer carbon nanomaterials from a dry bulk medium into airborne particles for delivery into a nose-only inhalation system. Utilization of a cannula-based feed system, diamond-coated wheel, aerosolization chamber, and krypton-85 source allows for delivery of otherwise difficult to produce respirable-sized particles. The particle size distribution (aerodynamic and actual) and morphology were characterized for different aerosolized carbon-based nanomaterials (e.g., single-walled carbon nanotubes and ultrafine carbon black). Airborne particles represented a range of size and morphological characteristics, all of which were agglomerated particles spanning in actual size from the nanosize range (<0.1 μm) to sizes greater than 5 and 10 μm for the particle's largest dimension. At a mass concentration of 1000 μg/m^3, the size distribution as measured by the inertial impactor ranged from 1.3 to 1.7 μm with a σ_g between 1.2 and 1.4 for all nanomaterial types. Because the aerodynamic size distribution is similar across different particle types, this system offers an opportunity to explore mechanisms by which different nanomaterial physicochemical characteristics impart different health effects while theoretically maintaining comparable deposition patterns in the lungs. This system utilizes relatively small amounts of dry material (<0.05 g/h), which may be beneficial when working with limited quantity or costly nanomaterials.

Received 25 August 2010; accepted 30 March 2011.

Research was funded by NIH grants RC1 ES018232 and U01ES020127, US EPA Star grants R831714, R832414, and R82215, NIOSH grant 0H07550, and Student Fellowship from the University of California Toxic Substances Research and Teaching Program of the University of California, Davis. We acknowledge the laboratory of Dr. Alexandra Navrotsky and the Nanomaterials in the Enviornment, Agriculture and Technology (NEAT) Organized Research Unit at the University of California, Davis for graciously providing the BET analysis of nanomaterials used in this study.

Address correspondence to Amy K. Madl, Center for Health and the Environment, University of California, One Shields Avenue, Davis, California 95616, USA. E-mail: akmadl@ucdavis.edu

INTRODUCTION

Nanotechnology provides promise for significant advancements in a number of different fields including imaging, electronics, and therapeutics (Drexler 1992; Hu et al. 1999; Alivisatos 2000; Navrotsky 2001; Smalley 2001; Lieber 2003; West and Halas 2003). While engineered nanoscale materials are already being utilized in a variety of applications (e.g., dispersive agents in cosmetics, composites in automotive parts, tubes in flat panel displays, and fibers in textiles), understanding the toxicological and biocompatible properties of these materials within a variety of settings (e.g., occupational, environmental, or consumer product) will become critical as new substances move from research and development into high-volume industrial production. Although inhalation exposure of nanomaterials would most commonly be thought of as an industrial or occupational hazard, researchers are exploring the delivery of engineered nanomaterials to the respiratory tract as a mechanism for diagnostics or targeted drug therapy. Possible biomedical applications of inhaled nanomaterials include enhanced antibiotic treatment of tuberculosis (Sung et al. 2009), chemotherapy of lung cancer (El-Gendy and Berkland 2009), whole-body imaging of particles deposited in the lungs using magnetic resonance imaging (Martin et al. 2008), and drug delivery to targeted regions of the lungs using magnetic fields against supramagnetic iron oxide nanoparticles (Dames et al. 2007). The use of nanomaterials as a drug carrier system and the delivery of these vehicles by inhalation are a possible approach to targeting drugs to the lungs. This therapeutic non-invasive approach would potentially offer high local drug concentrations that may lower therapeutic doses, reduce systemic effects, and reduce metabolic degradation of drugs in the liver

compared with oral or systemic treatment (El-Gendy and Berkland 2009; Sung et al. 2009). However, in order to understand the deposition, fate, and transport of nanomaterials that enter the respiratory tract and their potential for biocompatibility or toxicity, it is critical to have a means to deliver these aerosolized materials in experimental studies in a manner comparable with that experienced in different human exposure settings (e.g., inhalation).

Researchers have used a variety of different aerosolization systems to generate aerosols of nanomaterials. For example, a system encompassing an acoustic fluidization feeder, mill, and size separator was used to generate aerosolized single-walled carbon nanotubes (SW-CNTs; Baron et al. 2008), whereas a jet mill coupled to a dry chemical screw feeder (Mitchell et al. 2007) or a 6-jet collision nebulizer (Ryman-Rasmussen et al. 2008) was utilized to aerosolize multiwalled carbon nanotubes (MW-CNTs). Other test systems employed for generating nanomaterials have included a brush dust generator for inhalation studies of nanotitanium dioxide (Ma-Hock et al. 2009), as well as a direct delivery of aerosolized nanomaterials from an evaporation reactor (e.g., silicon dioxide; Ostraat et al. 2008) or combustion with a laminar diffusion flame system (e.g., ultrafine iron; Yang et al. 2001). Researchers have also compared the consistency, homogeneity, and size distribution of aerosols of nanomaterials generated by a variety of wet and dry aerosolization systems (Schmoll et al. 2009). Depending on the characteristics of the feedstock or bulk material used to generate the aerosol, some significant challenges can be faced in efficiently delivering a stable, well-characterized aerosol in a continuous manner. One such example is the aerosolization of SW-CNTs, which has a very low density, strong van der Waal force that promotes agglomeration and a high degree of flexibility and compression ability that can result in a highly compact structure that is difficult to dissociate (Baron et al. 2008).

In testing different wet and dry aerosolization systems for nanomaterials, none have been shown to produce an aerosol with a size distribution comparable with the primary particle size specified by the manufacturer. While wet methods (e.g., nebulizer) for nanomaterial aerosolization have been shown to produce a consistent aerosol concentration of sufficient magnitude, the resulting aerosol contains particles derived from the carrier water (Schmoll et al. 2009). Conversely, dry aerosolization methods in the Schmoll et al. study were unable to produce consistent aerosol concentrations, but SW-CNTs could be generated into loosely structured particulates with individual nanotubes being clearly visible by electron microscopy (rather than spheroid agglomerates by nebulization). Although most aerosolization methods are capable of producing agglomerate size distributions less than a geometric mean of 200 nm, aerosol morphology, composition concentration magnitude, and consistency can vary considerably depending on the selected nanomaterial and aerosolization system (Schmoll et al. 2009). Despite the difficulties with aerosolizing nanomaterials, there is still a strong need to develop aerosolization systems for toxicity studies and safety analyses. Therefore, for the purpose of this study, we pursued the design, development, and characterization of a dry aerosol system for carbon-based nanomaterials because (1) other studies have shown the successful delivery of carbon-based nanomaterials via dry bulk media, (2) potential airborne exposures during the initial handling of carbon-based nanomaterials produced in industrial settings involve dry bulk material, and (3) contaminants in suspension media for wet aerosolization may alter physical and chemical characteristics of aerosol test material making hazard analysis difficult to relate to industrial exposure settings or to compare with other nanomaterials.

SW-CNTs have received notable attention due to their superior electronic, optical, mechanical, chemical, and even biological properties. These materials show promise for a wide array of applications, including substrates for neuronal cell growth (Mattson et al. 2000; Hu et al. 2004; Lovat et al. 2005), scaffolding for tissue and bone growth (Usui et al. 2008), supports for liposaccharides to mimic cell membranes (Chen et al. 2004), ion channel blockers (Park et al. 2003a, 2003b), tumor imaging (Zavaleta et al. 2008), and drug delivery systems (Bianco and Prato 2003; Bianco et al. 2005a, 2005b, 2005c; Foldvari and Bagonluri 2008a, 2008b). In addition to their medical applications, carbon nanotubes are expected to advance electronics, within energy storage devices, thermal insulators, conducive fillers, and molecular electronic devices (Baughman 2000; Gao et al. 2000; Katz and Willner 2004; Bianco et al. 2005b, 2005c; Fortina et al. 2005). Because carbon nanotubes are projected to be incorporated into manufactured goods valued in the trillions over the next 5–10 years, there is a potential for human exposure in industrial settings and a strong need to understand the potential health effects of these materials.

Several inhalation studies of MW-CNTs have been conducted; however, only one study has focused on the effects of SW-CNTs (Shvedova et al. 2008). Some of the challenges faced in aerosolizing both MW-CNTs and SW-CNTs include particle agglomeration and the relatively low efficiency in delivering an aerosol in the respirable size range to the animal exposure chamber (Baron et al. 2008), which results in relatively large quantities of bulk material being required to meet the target aerosol concentration (Mitchell et al. 2007; Baron et al. 2008). Because new nanomaterials may only be produced in small quantities during the research and development phase, researchers could utilize an approach for toxicity and hazard comparison studies to deliver relatively small quantities of different nanomaterials by inhalation with similar aerodynamic aerosol properties.

The purpose of this study was to develop an aerosolization system for administration of nanomaterials from a dry bulk medium into an aerosol encompassing airborne particles within the respirable size range for delivery into a nose-only inhalation system. This system was tested with carbon nanotubes, because of its array of potential industrial, therapeutic, and consumer product applications and the need to evaluate the effects of these materials via inhalation, an exposure route anticipated for occupational settings. Comparing the health effects of engineered nanomaterials (i.e., SW-CNTs) with other nanoparticles

(i.e., carbon black) for which the toxicity is more well established and better understood can be useful in ranking the potential hazards or risks posed by newly produced nanomaterials. Thus, an additional objective of this study was to characterize the size, shape, and morphology of aerosolized SW-CNTs of different chemical formulations and to evaluate the feasibility of aerosolizing nanosized carbon black within the same aerosolization system for future toxicological comparison studies of carbon-based nanomaterials.

METHODS

Nanomaterials

SW-CNTs were obtained from Unidym (formerly Carbon Nanotechnologies, Inc., Houston, TX). These nanomaterials were produced by high-pressure carbon monoxide (HiPCO) disproportionation process using carbon monoxide as the carbon feedstock and iron pentacarbonyl as a metal catalyst. Characteristics that were reported by the manufacturer indicated that the SW-CNTs contained less than 35 wt% ash content and 25 wt% residual iron catalyst. Residual metal catalyst was removed from the iron-containing SW-CNTs (hereafter referenced as FeSW-CNTs) according to the methodology described by Wang et al. (2007), which involved heating the FeSW-CNTs at 40°C–70°C in an aqueous mixture of hydrogen peroxide and hydrochloric acid leaving clean or purified SW-CNTs (hereafter referenced as cSW-CNTs). This purification process combines two known reactions: oxidation of carbon nanotube materials by hydrogen peroxide and removal of metals by hydrochloric acid (Wang et al. 2007). Bulk analysis (described below) was conducted to verify the metal content, as well as the purity of the FeSW-CNTs and cSW-CNTs. Nanocarbon black (Monarch 120) was obtained by the Cabot Corporation (Billerica, MA) and was reported by the company to contain 100% elemental carbon. This carbon black consists of primary particles with a mean diameter of 75 nm and the smallest dispersible aggregates of physical diameters ranging from 150 to 200 nm (Cabot Corporation). Impurity and surface area analyses as performed for the SW-CNTs were also conducted for the bulk carbon black.

Aerosolization System

The aerosolization system generally consisted of a cannula-based feeder, diamond-coated wheel, aerosolization chamber, and a krypton-85 aerosol electrostatic discharger (Figure 1). The nanomaterials were loaded and packed into a cannula that served as the "hopper," from which the nanomaterials were continuously fed into the aerosolization chamber. Although a couple of cannulas were initially tested and determined to work well with the system (first an 11-gauge stainless steel surgical cannula and then a similar sized biopsy needle), brass tubes (3.5 mm internal diameter × 4 mm outside diameter; Grainger, Inc., Bethel, CT) cut to 80 mm length were found to be most optimal due to the metal strength and tube diameter. Specifically, the brass tube appeared to be resistant to bending while the material was being advanced through the "hopper" by the plunger (Grainger, Inc.) and offered a larger internal diameter that would result in a shorter, larger diameter plug of nanomaterials, which was less prone to being jammed. The diamond-coated wheel (Grainger, Inc.) sheared the face of the packed nanomaterials as they were advanced from the cannula into the aerosolization chamber. The authors found that packing the bulk material into a dense plug of about 1 cm in length in the cannula by hand pressure was optimal for this system. Each cannula was manually packed by loading the nanomaterials through a custom machined plastic funnel (Teague Enterprises, Woodland, CA) that would allow the material to be pushed into the cannula with a long needle. Once a sufficient amount of nanomaterials was loaded into the cannula, the plunger (which is used to advance the nanomaterial plug during aerosolization) was used to pack the material against a hard surface and form a dense plug within the cannula. This process was repeated several times until an approximate 1-cm plug of nanomaterials was loaded in the cannula.

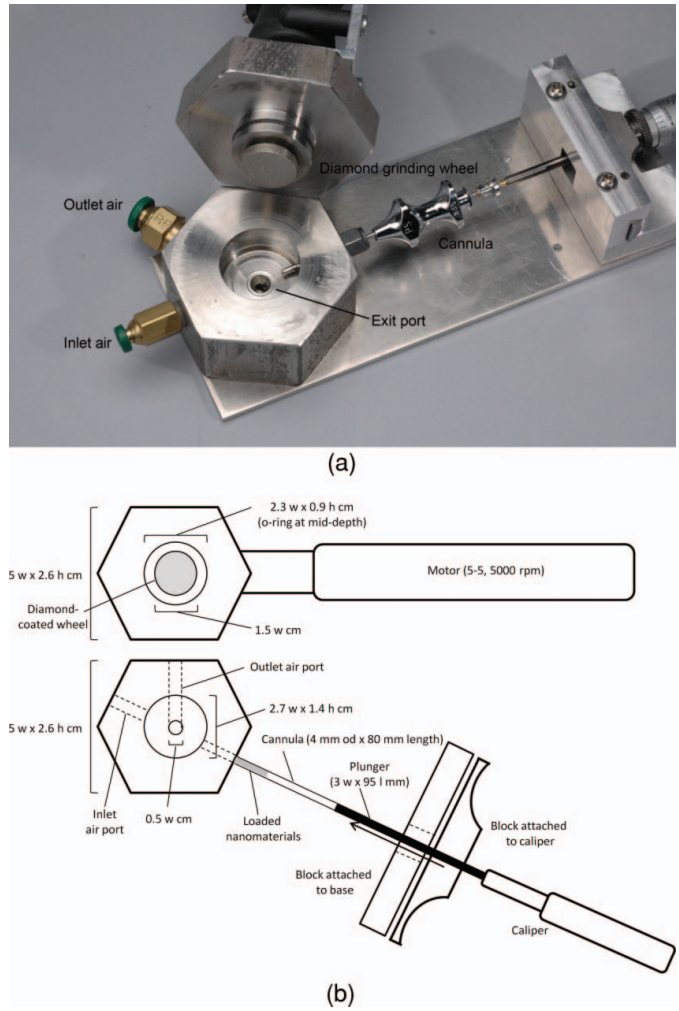

FIG. 1. (a) Photo and (b) diagram illustrating components and measurements of the nanomaterial aerosol generation system. (Color figure available online.)

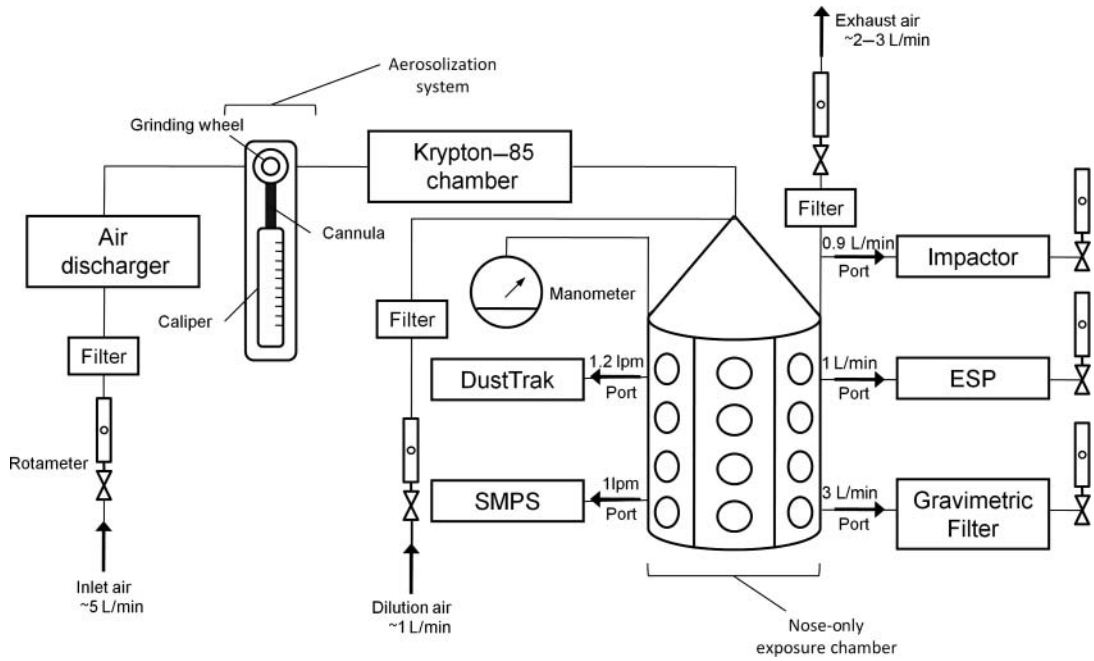

FIG. 2. Diagram of aerosolization and nose-only inhalation system.

The aerosolization chamber was made of stainless steel (Blue Collar Supply, Sacramento, CA) and was machined to the dimensions outlined in Figure 1 (Teague Enterprises, Woodland, CA). The aerosolization chamber consisted of an internal cylindrical chamber that contained access ports so that nanomaterials and makeup air [5 liters per minute (L/min) maintained at a constant rate for all target concentrations] could be simultaneously introduced into the system. A diamond-coated wheel, positioned in the center of the chamber, sheared the plug of nanomaterials that were advanced from the cannula. The diamond-coated wheel was operated by a rotary motor tool with ratings between 5 and 35,000 rpm, but was operated during aerosolization at approximately 5000–5500 rpm (Dremel, Grainger, Inc., Bethel, CT). A static discharger (Model 1055, Meech Static Eliminator, Richfield, OH) was attached in line immediately before the aerosolization chamber as a means to reduce the charge generated as the nanomaterials were advanced into the aerosolization chamber and sheared by the diamond-coated wheel. While this device did not seem to make a measurable difference by enhancing the delivery of aerosolized nanomaterials, it was maintained in line, nonetheless, during the aerosolization as a means to potentially minimize the charges generated during the aerosolization process. With the circular motion of the diamond-coated wheel and the introduction of makeup air, the aerosolization chamber retained visibly larger particles in the chamber and allowed smaller particles to exit the chamber through a port at the bottom of the chamber (Figure 1). The aerosolized particles were fed through a krypton-85 source to reduce the electrostatic charge to Boltzmann equilibrium, minimize reaggregation of aerosolized particles, and maximize delivery to a nose-only inhalation exposure chamber (Figure 2). Initial tests of the aerosolization system showed that without the krypton-85 source, measurable mass concentration of aerosolized nanomaterials could not be detected in the nose-only inhalation chamber. Although the entire aerosolization and exposure system was a closed system, it (aerosolization system, krypton-85 source, optical particle counter [DustTrak, TSI, Inc., Shoreview, MN], and nose-only inhalation chamber) was set up and maintained in a containment area with active ventilation to prevent any release to the laboratory workspace.

It is noteworthy that initial attempts to aerosolize SW-CNTs included the use of a similar system except with a brush wheel attachment rather than a diamond-coated wheel, as well as an entirely different system (a vibrating fluidized bed of glass beads) that has been successful in aerosolizing archived fine and coarse particulate matter (Teague et al. 2005). Both of these attempts were not entirely successful. Although the brush wheel attachment produced aerosolized particles, some of the particles appeared as dense flakes that were morphologically uncharacteristic of SW-CNTs. With the fluidized glass bead system, the electrostatic characteristics of the SW-CNTs caused these particles to remain adhered to the glass beads, and as a result, no aerosolized particles were generated.

Bulk Analysis

Bulk samples of FeSW-CNT, cSW-CNT, and carbon black were analyzed for iron by inductively coupled plasma mass spectroscopy (ICP-MS) according to US Environmental Protection Agency (US EPA) IO Method 3.4 (US EPA 1999) and surface area by thermal adsorption–desorption isotherms of nitrogen by

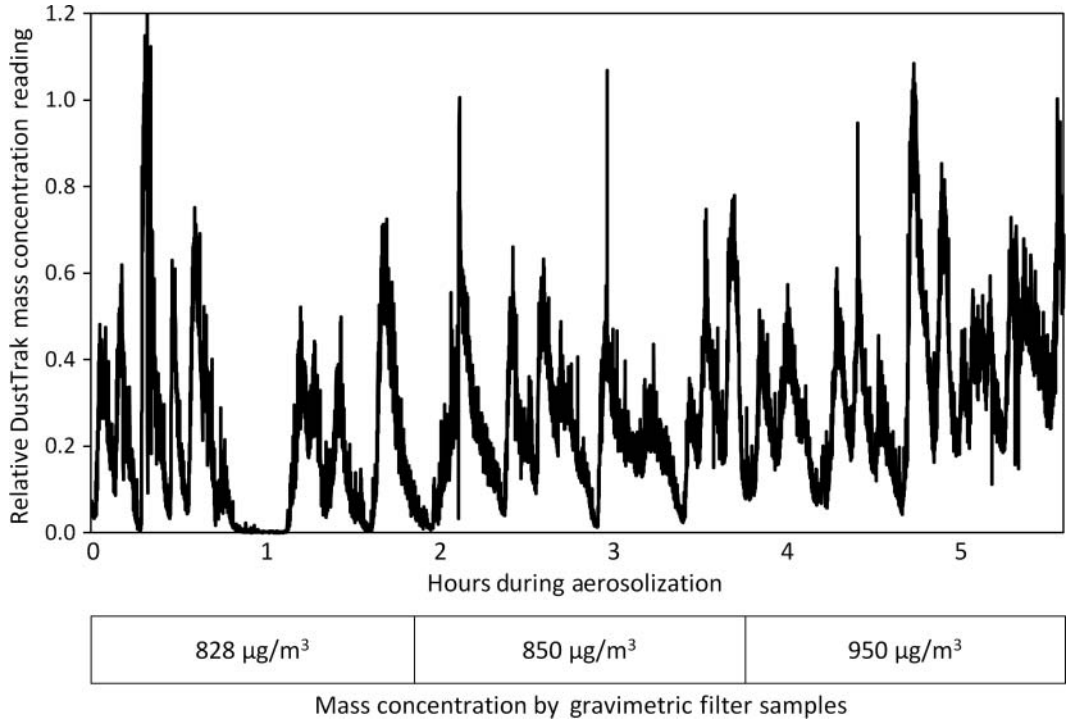

FIG. 3. Real-time DustTrak reading during aerosolization of FeSW-CNT at ∼1000 μg/m^3.

the Brunauer, Emmett, and Teller method. Surface area measurements were only collected for the bulk material because sufficient masses of aerosolized carbon nanomaterials could not be collected to meet the detection limits of this method.

Aerosol Monitoring and Characterization

Carbon nanomaterials (FeSW-CNT, cSW-CNTs, and carbon black) were aerosolized and continuously delivered to a nose-only exposure chamber for 6 h (Figure 2). Aerosolized nanomaterials from inside the nose-only exposure chamber were continuously measured with a TSI DustTrak (TSI, Inc.) equipped with a PM10 impactor and operated at an airflow rate of 1.2 L/min to allow for real-time adjustment of mass concentrations within the nose-only exposure chamber. Readings obtained from the DustTrak are relative, because the mass concentrations (rated to measure particles between 0.1 and 10 μm in diameter) are calibrated to a standard model particle by the manufacturer. Therefore, DustTrak readings were only used to understand the real-time dynamics of the aerosol in the nose-only exposure chamber and prompt the operator when to advance the bulk material into the aerosolization chamber so the target concentration (measured by gravimetric filters) can be met. Mass concentrations of the aerosol were characterized by gravimetric filter measurements, which were time weighted over the sample duration and determined with a microbalance (M5P Filter Microbalance, Satorius, Goettingen, Germany). The minimum or threshold DustTrak reading that would prompt the advancement of the bulk material and correspond to an average target mass concentration (measured gravimetrically) was determined a priori and differed based on the nanomaterial being aerosolized. Figure 3 illustrates the real-time dynamics and fluctuations of the aerosol, even though the gravimetric filter measurements are stable and consistent (as described in the Results section). Over the entire duration of the aerosolization of SW-CNTs, consecutive gravimetric filter measurements of particles collected from within the exposure chamber were taken at an airflow rate of 3 L/min with preweighted filters (borosilicate glass microfibers reinforced with woven glass cloth and bonded with polytetrafluoroethylene, Pallflex membrane filters, Pall Life Sciences, East Hills, NY). Figure 3 illustrates the fluctuation of DustTrak readings and adjustment required to meet a target concentration of approximately 1000 μg/m^3.

The particle number concentration and size distribution were monitored in real time with a scanning mobility particle sizer (SMPS, TSI, Inc.) system composed of a condensation particle counter (CPC; Model 3010, TSI, Inc.) in line with a differential mobility analyzer (Model 3081, TSI, Inc.). SMPS measurements were collected for 120 s throughout the 6 h aerosolization at an airflow and a sheath flow rate of 1 and 1 L/min, respectively. The size distribution of aerosolized nanomaterials was characterized by the SMPS for particles between the size range of 27 and 1000 nm. The inertial particle size distribution was assessed with a Mercer seven-stage cascade impactor (In-Tox Products, Albuquerque, NM) with inertial cutoff points ranging from 0.22 to 3.4 μm. To assess the aerodynamic size distribution of the different aerosolized

carbon-based nanomaterials, impactor samples were collected at an airflow rate of 0.9 L/min and the median mass aerodynamic diameter (MMAD) was measured gravimetrically, as well as by a thermal-optical analyzer for total carbon in accordance with the NIOSH method 5040 to estimate the relative mass portion of nanomaterials deposited on each impactor stage. Respirable particles were defined in accordance with the British Standards Institution (BSI) and by the International Organization for Standardization (ISO) that is relied upon by the American Conference of Governmental Industrial Hygienists (ACGIH; BSI 1993; ISO 1995). These organizations define respirable-sized particles as those with an aerodynamic diameter given by a cumulative lognormal distribution with a median diameter of 4.25 μm and a geometric standard deviation of 1.5.

Aerosolized SW-CNTs were analyzed for purity and carbon structural allotropy by Raman spectroscopy. Raman spectra were acquired of aerosolized nanomaterials collected on different impactor stages using a diode-pumped Nd:YAG laser (Millenium 5W, Spectra-Physics) operating at 532 nm as the excitation source, a Raman microscope with a long-pass filter (used twice to reject the excitation laser line while allowing the Raman scattering light to pass) and 63× objective (Zeiss, ACHROPAN, 0.80 NA), a charge-coupled device (CCD) detector (EEV 256 × 1024, Princeton Instruments, Trenton, NJ), and spectrometer (Acton Pro 300i) with 600 L/mm grating blazed for 532 nm. To optimize the signal-to-noise ratio, spectra were acquired using three scans of 50 s for each spectral region and ~1% of the laser source power and fully focused laser beam. The software Winspec32 by Princeton Instrument was used to analyze the spectra. The Raman spectra were taken in the frequency range up to 2568 cm^{-1}.

The size, morphology, and chemistry of aerosolized SW-CNTs and carbon black were analyzed by transmission electron microscopy (TEM). Aerosolized nanomaterials were collected on carbon-coated copper grids (carbon on Formvar grid 200 mesh copper, Ted Pella, Inc., Redding, CA) with an electrostatic precipitator (Teague Enterprises, Woodland, CA) operating at an airflow rate of 1 L/min. While the SMPS measurements were collected in real time and directly from the nose-only exposure chamber, the impactor and TEM grid samples were also collected from a port in the exposure chamber but analyzed off-line.

TEM and energy dispersive spectroscopy (EDS) were used to visualize the size distribution and morphology of aerosolized particles as well as to measure the metal content of individual particles. Work was performed on either a JEOL JEM-2100F or a JEOL 2500SE. The 2100F was operated in TEM mode under low-dose conditions with a 200 kV acceleration voltage and nominal magnifications ranging from 50× to 250,000×. Images were acquired on a 4096 × 4096 pixel TVIPS TemCam-415 CCD (Gauting, Germany). The 2500SE was used in scanning TEM (STEM) mode with a 200 kV acceleration voltage and 20,000× magnification. The EDS analyses were conducted with a Noran System Six EDS detector and software suite (Thermo Fisher Scientific, Inc., Waltham, MA). The size of the STEM probe was set to 0.5 nm. The spectra were analyzed using the Cliff–Lorimer method to determine the weight% and atomic%.

RESULTS

Aerosolization System

An aerosolization system was developed to administer nanomaterials from a dry bulk medium into airborne particles (median cut size less than 4.25 μm aerodynamic diameter) for delivery into a nose-only inhalation system. It was shown through continuous use of this aerosolization system that only small amounts of carbon nanomaterials are required to maintain concentrations up to 1000 $\mu g/m^3$. Figure 3 illustrates that by monitoring dust concentrations in real time with the DustTrak and advancing the nanomaterials into the aerosolization chamber as needed so that a consistent targeted mass concentration can be achieved. Using this real-time monitoring approach, airborne particle concentrations up to 1000 $\mu g/m^3$ of three different carbon nanomaterials (FeSW-CNT, cSW-CNTs, and carbon black) have been achieved. To generate an aerosol concentration of ~300 $\mu g/m^3$ (204 ± 176 $\mu g/m^3$ FeSW-CNTs and 292 ± 43 $\mu g/m^3$ cSW-CNTs as measured by gravimetric filter analysis) for a period of 6 h, approximately 0.015 g/h FeSW-CNTs and 0.008 g/h cSW-CNTs were required, whereas an aerosol concentration of 1000 $\mu g/m^3$ (916 ± 49 $\mu g/m^3$ FeSW-CNTs and 1167 ± 78 $\mu g/m^3$ cSW-CNTs) required approximately 0.05 g/h FeSW-CNTs and 0.025 g/h cSW-CNTs of the bulk material. On the basis of the amount of bulk material utilized or loaded in the system over a 6 h aerosolization and the resulting concentration in the exposure chamber, the estimated efficiency of delivery of aerosolized nanomaterials was approximately 0.6% for FeSW-CNTs, 1% for cSW-CNTs, and 3% for carbon black.

TABLE 1
Summary of bulk and aerosolized carbon nanomaterial characteristics

	Bulk material		Aerosolized particles at 1000 $\mu g/m^3$ Aerodynamic diameter	
	Fe (% by wt)[a]	SA (m^2/g)[a]	MMAD (μm)[b]	σ_g^b
FeSW-CNT	22.8	578	1.3	1.3
cSW-CNT	1.1	155	1.7	1.2
Carbon black	0.004	35	1.5	1.4

Note: SA, surface area.
[a]Measurements based on bulk sample analysis.
[b]Measurements collected from an inertial cascade impactor for particles in the range of 0.2–3.4 μm.

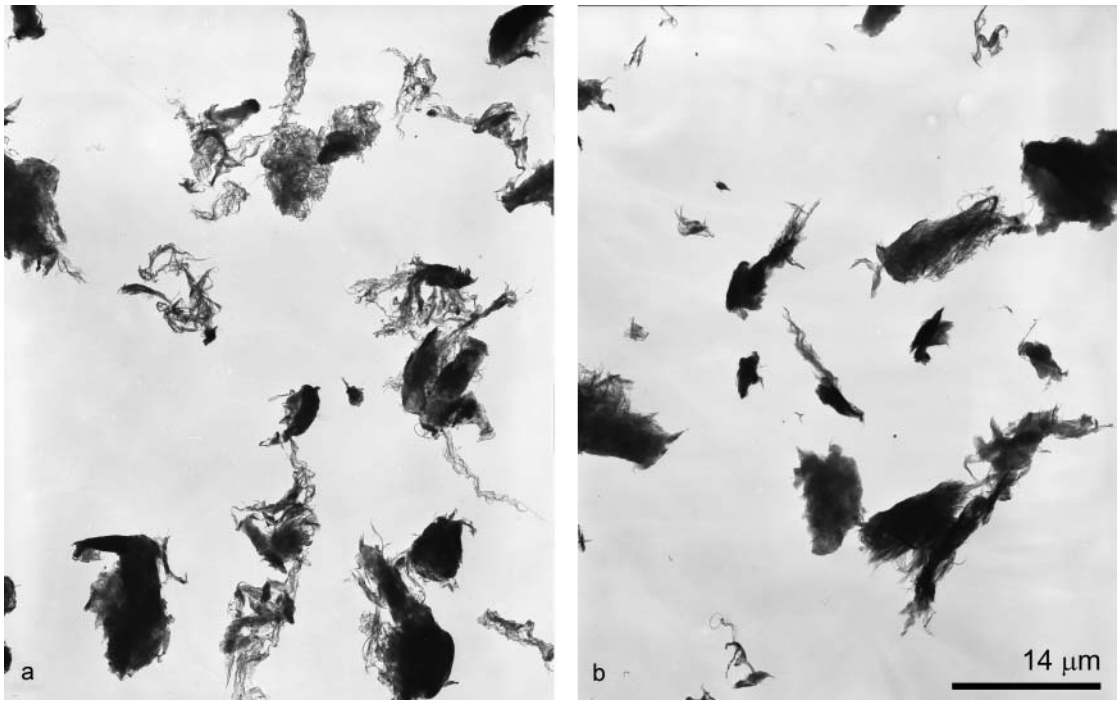

FIG. 4. TEM micrographs of aerosolized (a) FeSW-CNTs and (b) cSW-CNTs.

Bulk Analysis

Although FeSW-CNTs, cSW-CNTs, and carbon black are all carbon-based nanomaterials, their bulk characteristics vary considerably (Table 1). The purification process of FeSW-CNTs reduced the iron content from 22.8% to 1.1% by weight and very little (0.004%) iron was associated with the nanocarbon black. The surface area of the different nanomaterial types was also significantly different. The surface area for FeSW-CNTs (578 m^2/g) was greater than that observed for cSW-CNTs (155 m^2/g), most likely attributed to the purification process that resulted in a more compact bulk material. The surface area of the carbon black nanomaterials was significantly less (35 m^2/g) than that observed with the FeSW-CNTs or cSW-CNTs.

Aerosol Characteristics

Although the density, surface area, and iron content of the bulk material were significantly different across the different carbon nanomaterial types, the aerosol characteristics appeared to be comparable. At a mass concentration of 1000 $\mu g/m^3$, the size distribution as measured by the inertial impactor ranged from 1.3 to 1.7 μm with a σ_g between 1.2 and 1.4 for all nanomaterial types (Table 1). The particle size distributions, as measured by the SMPS during the nanomaterial aerosolization, were similar for all particle types (carbon black, FeSW-CNTs, and cSW-CNTs) and were not significantly different from background measurements prior to the aerosolization or from measurements collected with an impactor in line with the SMPS during aerosolization. It should be noted that no measurable background particulates were detected in gravimetric filter or impactor samples. Aerosolized particles of each type (FeSW-CNT, cSW-CNTs, and carbon black) were analyzed for size, morphology, and chemical composition by TEM equipped with EDS. Visualization of SW-CNTs by TEM showed a wide variation in sizes as well as fibrous and compact characteristics (Figure 4). Aerosolized FeSW-CNTs appeared more fibrous and open lattice in nature, whereas the cSW-CNTs were more dense and compact; the different morphological characteristics of the FeSW-CNTs and cSW-CNTs particles may be attributed to the fact that the cSW-CNTs underwent wet chemical processing. Because of the diverse morphology of the SW-CNTs, it was not feasible to devise a classification scheme to characterize these particles according to a specific shape (bundle, rope, or cluster) or aspect ratio. For example, there was no distinct fiber or rod-like structure of the SW-CNTs that would allow for the consistent measurement of width and length, and therefore, it was not possible to collect information on aspect ratios (the ratio of length to width). Instead of utilizing a specific classification scheme, the particle dimensions were measured according to the overall agglomerated structure, as well as substructures of individual SW-CNT strands. Agglomerated particle sizes as measured by TEM ranged from greater than 10 μm to less than 0.07 μm for the particle's largest dimension; however, most agglomerated structures were between 1 and 2 μm in overall size for carbon black and cSW-CNTs and slightly larger (2–4 μm in overall size) for FeSW-CNTs (Figure 4).

Although all aerosolized particles were agglomerated, SW-CNTs strands could be visualized within the complex mesh-like structures; these individual SW-CNTs were of a

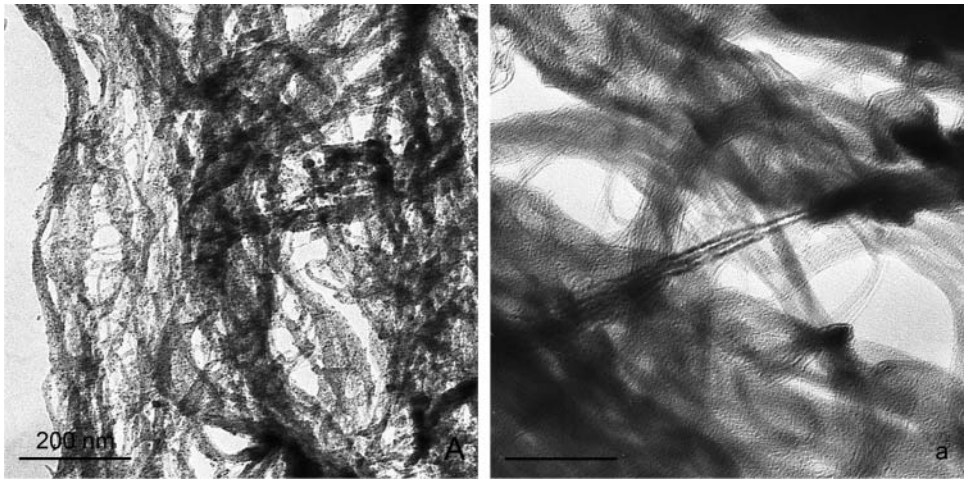

FIG. 5. TEM micrographs of aerosolized (a) FeSW-CNTs and (b) cSW-CNTs illustrating the morphology and presence or absence of residual iron catalyst nanoparticles.

dimension of approximately 4–10 nm in width (Figures 5 and 6). TEM imaging of these carbon particles proved to be challenging particularly to illustrate the finest morphological features of these particles because of a lack of contrast between the particles themselves and the carbon coating on the TEM grid. However, Figure 6 illustrates some of the smallest aerosolized particles that were collected during the aerosolization. Even at these smallest dimensions, the particles existed in an agglomerated state. Carbon black appeared as an agglomerated chain of smaller irregularly shaped spheres, FeSW-CNTs existed as a loose tangled "bird's nest" mat of individual and bundled CNTs, while cSW-CNTs appeared as smooth, blocky, torn sheets with individual and bundled CNTs only visualized at the very edges of the agglomerated particles (Figure 6).

Aerosolized FeSW-CNT, cSW-CNT, and carbon black were analyzed by Raman spectroscopy. It was observed that the purification of SW-CNTs with a mixture of H_2O_2 and HCl had a significant effect on the SW-CNTs as shown by the Raman spectra. The D band, which is related to the sp^3 carbon cluster in the graphite sheet and can be an indication of structural defects in the crystallinity of the tubes or the presence of amorphous carbon, was significantly reduced in magnitude for the sample following purification. In contrast, there was a considerable shift of the G band frequency following purification, from two peaks at 1539 and 1592 cm^{-1} for the FeSW-CNTs to a broad single peak at 1573 cm^{-1} for the cSW-CNTs (Figure 7, Table 2; not deconvoluted). The intensity ratio of the D and G bands (I_D/I_G) is a tool used to monitor the amorphous carbon content and density of carbon bond defects of SW-CNTs. The purification caused the intensity ratio of the D and G bands to decrease for the cSW-CNTs suggesting a removal of amorphous carbon without a significant introduction of sidewall defects from the H_2O_2/acid treatment. The Raman spectra for carbon black showed broad D and G bands and a high intensity ratio (I_D/I_G) of these bands, which are characteristic of carbon black and disordered graphitic bonds.

TABLE 2
Raman band frequency for aerosolized SW-CNTs and carbon black

	Raman band frequency/cm^{-1}		
	D	G	I_D/I_G
FeSW-CNT	1332	1539/1592	0.35
cSW-CNT	1332	1573	0.19
Carbon black	1350	1590	0.97

TEM imaging illustrated and confirmed the removal of electron-dense iron nanoparticles following acid treatment and purification that had originally decorated the surface of the FeSW-CNTs (Figure 8). Although ICP-MS analysis indicated that approximately 1% of iron still remained in the cSW-CNT samples (Table 1), both TEM imaging (Figures 5 and 6) and EDS analysis (Figure 8) showed that very little iron was present. There was also some variability in the iron content of aerosolized SW-CNTs with average concentrations of 11.67 wt% Fe (range 1.76–32.97 wt% Fe) and 1.00 wt% Fe (range 0–6.99 wt% Fe) observed for FeSW-CNTs and cSW-CNTs, respectively. It should be noted, however, that the iron content of the cSW-CNTs is near the analytical limit of detection for EDS and, as a result, may offer limited information about the residual metals present with the cSW-CNTs.

DISCUSSION

A unique and relatively simple aerosolization system was designed to generate a respirable aerosol of nanomaterials for use in nose-only inhalation toxicity studies. This system offers several advantages. First, only small mass amounts of SW-CNT

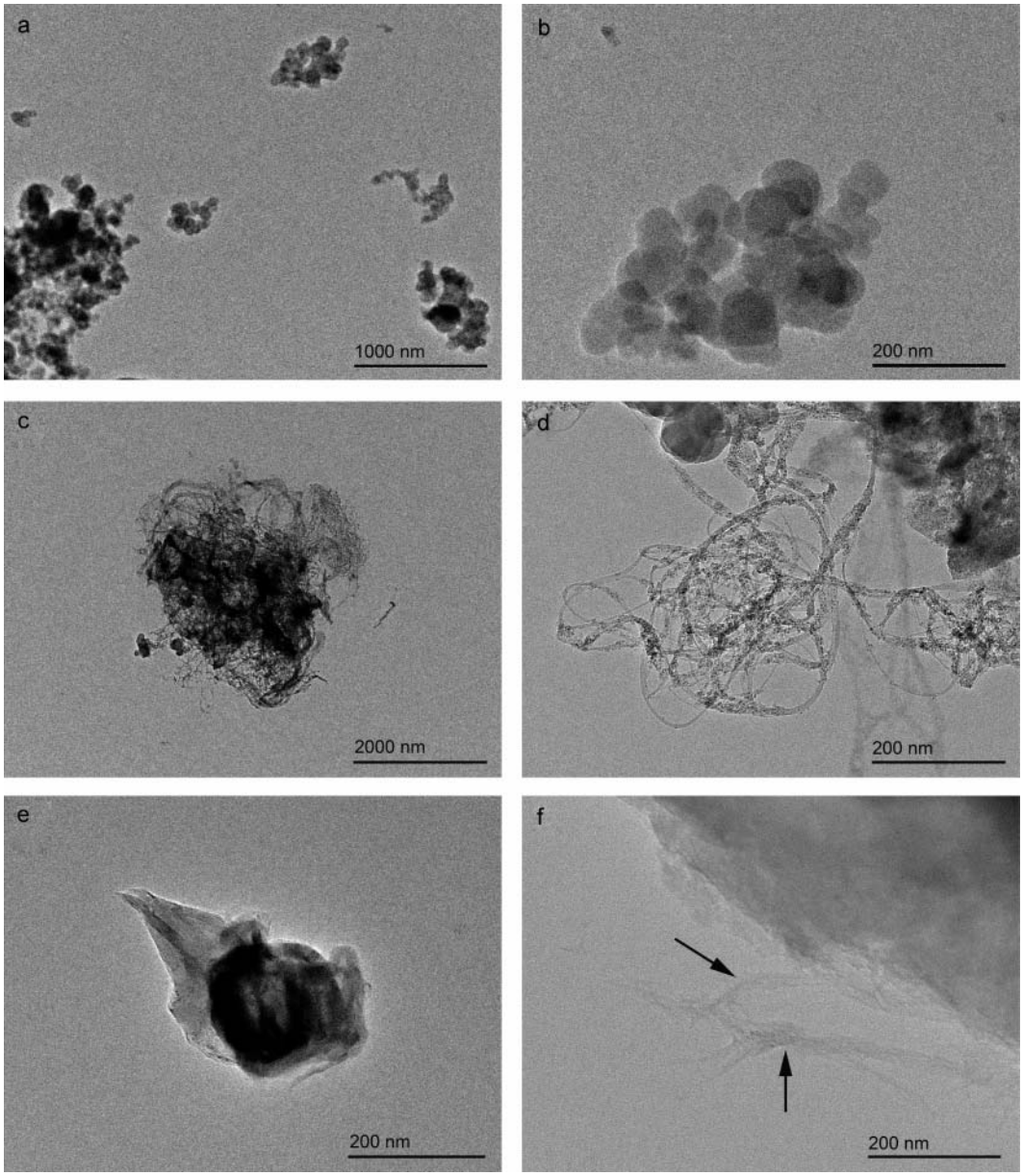

FIG. 6. TEM micrographs illustrating the morphology and substructures of some of the smallest aerosolized particles of (a, b) carbon black, (c, d) FeSW-CNTs, and (e, f) cSW-CNTs. At the smallest dimensions, these particles existed in an agglomerated state. (a, b) Carbon black appeared as an agglomerated chain of smaller irregularly shaped spheres, (c, d) FeSW-CNTs existed as a loose tangled "bird's nest" mat of individual and bundled CNTs, while (e) cSW-CNTs appeared as smooth, blocky, torn sheets with individual and bundled CNTs only visualized at the very edges of the agglomerated particles (shown in arrows in f).

were needed for a continuous exposure to concentrations up to 1000 μg/m^3. This characteristic of the aerosolization system is particularly important for materials that can only be produced in small quantities or are costly. Thus, the effective delivery of aerosolized particles offers an opportunity for inhalation studies of nanomaterials that may normally be prohibitive by cost or availability. Second, inertial size distributions are relatively similar across different types of nanomaterials, which may be useful in hazard comparison studies. The analysis of bulk and air samples shows that there are significant chemical (Fe and amorphous carbon content and carbon crystallinity) and physical (density, surface area, and morphology) differences between FeSW-CNTs, cSW-CNTs, and carbon black, whereas the aerodynamic aerosol characteristics are similar. Because the aerosol size distribution is similar across different particle types, this system offers an opportunity to explore mechanisms by which different nanomaterial physicochemical characteristics impart different health effects while theoretically maintaining comparable deposition patterns in the lungs. Therefore, the roles that particle surface area, morphology, iron content, and carbon

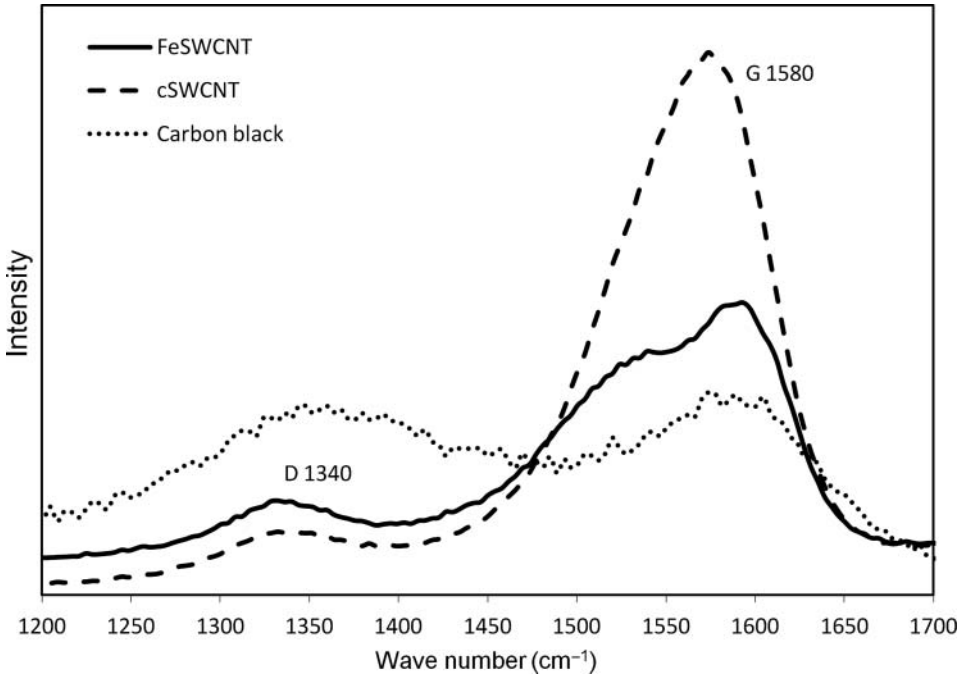

FIG. 7. Raman spectra of aerosolized carbon nanomaterials. Spectra profile represents the relative and not the absolute intensity of the Raman peak measurements of the different samples to interpret the structural composition.

bonding of carbon nanomaterials have in influencing toxicity or biocompatibility can be explored within specific regions of the respiratory tract receiving comparable doses.

Although the density, surface area, and iron content of the bulk material were significantly different across the different carbon nanomaterial types, the aerosol characteristics appeared to be comparable. At a mass concentration of 1000 μg/m^3, the size distribution as measured by the inertial impactor ranged from 1.3 to 1.7 μm with a σ_g between 1.2 and 1.4 for all nanomaterial types (Table 1). The particle size distributions, as measured by the SMPS during the nanomaterial aerosolization, were similar for all particle types (carbon black, FeSW-CNTs, and cSW-CNTs) and were not significantly different from background measurements prior to the aerosolization or from measurements collected with an impactor in line with the SMPS during aerosolization. Although there were aerosolized particles less than 1 μm in diameter (particularly with aerosolized carbon black) identified by TEM, the inability of the SMPS to detect aerosolized particles may be a result of either the number of particles in this size range being so small that it is indistinguishable from background or there may be some nanomaterial characteristics (e.g., electrophysical) that may interfere with the charge and diffusion properties within the SMPS. For example, it has been suggested that fibrous carbon materials, such as carbon nanotubes, can have much larger physical diameters than their mobility diameters and may bypass the impaction plate, which normally removes larger-sized particles, and cause disruption in the electric and flow field inside the classifier (Ku et al. 2007). Although no anomalous voltage fluctuations were observed in our measurements, it has been proposed that fibrous carbon nanomaterials may cause arcing as a result of particles being deposited on the differential mobility analyzer (DMA) electrode surface or by mixing of aerosol and sheath flows by either corona wind or particles moving back and forth as they travel downward in the DMA (Ku et al. 2007).

There are few studies that have developed aerosolization systems and delivered carbon-based nanomaterials via inhalation (Li et al. 2007; Mitchell et al. 2007; Ryman-Rasmussen et al. 2008; Shvedova et al. 2008). In the Mitchell et al. (2007) study, MW-CNTs were aerosolized with a jet mill coupled to a dry chemical screw feeder and a 2-μm cut-point cyclone. For MW-CNTs concentrations of 500–1000 μg/m^3, these authors report an MMAD of approximately 0.7–1 μm ($\sim$2.0 geometric *SD*) and a median particle number size distribution of approximately 350–400 nm. The MMAD increased to 1.8 μm (2.5 geometric *SD*) for the 5000 μg/m^3 exposure. Although the efficiency of delivery of MW-CNTs within this aerosolization and entire exposure system was not reported, it was noted that 100 g of MW-CNTs was utilized for the study, which involved three different concentration levels (300, 1000, or 5000 μg/m^3) and two durations of exposure (6 h/day for 7 or 14 days; Mitchell et al. 2007). In comparison, aerosolized SW-CNTs generated by an acoustic fluidization feeder, mill, and size separator at a mass concentration of 5000 μg/m^3 exhibited an MMAD of 4.2 μm [based on the iron content of filters from various stages of a micro-orifice uniform deposit impactor (MOUDI)] and a count mode aerodynamic diameter of approximately 240 nm (based on counting micrographs of MOUDI stages with a cutoff of 0.18 μm; Baron

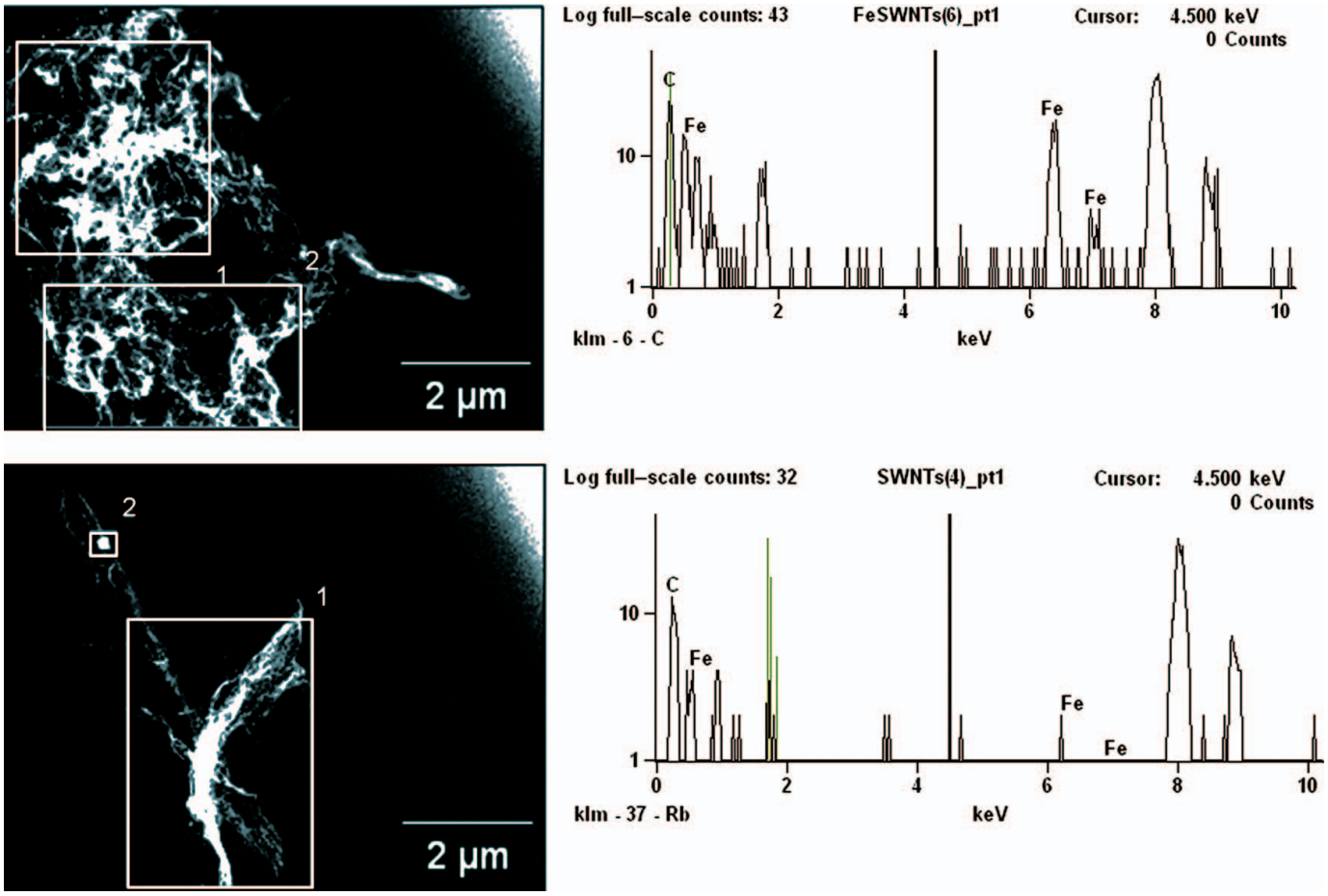

FIG. 8. TEM micrographs and EDS spectra of aerosolized (a) FeSW-CNTs and (b) cSW-CNTs illustrating the morphology and presence or absence of residual iron catalyst nanoparticles. Squares in the images represent the area over which the EDS spectra were analyzed for the elemental composition of aerosolized nanomaterials. The elemental profile as shown in the EDS spectra on the right represents the area analyzed in square 1 of the TEM images shown on the left. (Color figure available online.)

et al. 2008; Shvedova et al. 2008). Although the original amount of bulk SW-CNTs that was utilized in the aerosolization was not reported, an output efficiency of 10%–12% was noted based on the mass of material at the output and the mass of material collected in the settling chamber and first cyclone (Baron et al. 2008). However, the amount of SW-CNTs loaded into the hopper was not reported or compared with the amount that ultimately entered the exposure chamber, which is the necessary information to make side-by-side efficiency comparisons to our aerosolization system. Even though a 1%–3% efficiency from the cannula-based hopper to the nose-only exposure chamber from our system is not ideal, it is not far from the aerosolization efficiencies reported for other systems of archived particulate matter (Teague et al. 2005). Furthermore, based on data that we collected, a 10-day exposure study (6 h/day) would only require 3 g of SW-CNTs, which is still a relatively small amount compared with that utilized in the Mitchell et al. (2007) study.

There have been a number of hypotheses offered regarding possible mechanisms by which CNTs can be toxic. It has been proposed that the type of carbon nanomaterial (i.e., SW-CNT, MW-CNT, and fullerene), method of production (i.e., chemical vapor deposition, arc discharge, and laser ablation), extent of purity (i.e., refined or unrefined), presence of residual transition metal catalysts, functionality of different reactive groups, dimension, and method of administration can influence the health effects observed with these nanomaterials (Lam et al. 2004; Muller et al. 2005; Dumortier et al. 2006; Magrez et al. 2006; Tian et al. 2006; Sayes et al. 2007; Muller et al. 2008; Poland et al. 2008; Shvedova et al. 2008; Tong et al. 2009). One novel characteristic, however, that has gained some consideration is the potential role of carbon bond defects and acid functional groups in eliciting inflammatory and fibrotic responses with exposure to MW-CNTs (Muller et al. 2008). These different physicochemical characteristics are important because manipulating the chemistry of CNTs, as well as the

dispersive agents used to solubilize them, can have dramatic effects on the clearance and retention of these nanomaterials (Singh et al. 2006; Schipper et al. 2008). Further, functionalization of SW-CNTs with water-soluble functional groups can influence cellular-specific uptake, tolerance by primary immune cells, and induction of oxidative stress and apoptosis in a variety of cell systems (Cui 2005; Ding et al. 2005; Jia et al. 2005; Manna et al. 2005; Monteiro-Riviere et al. 2005; Bottini et al. 2006). Given the diverse physicochemical characteristics of carbon nanotubes, utilizing an aerosolization system whereby nanomaterials of different chemical and morphological characteristics can be delivered with similar aerosol properties in experimental animal inhalation studies would be tremendously helpful in hazard comparison studies and in delineating which physicochemical characteristics dictate the difference between toxicity and biocompatibility.

Grinding, heating, and purification can have an effect on the surface chemistry and size distribution of SW-CNTs (Shen et al. 2005; Fenoglio et al. 2008). For example, acid treatment can remove amorphous carbon, reduce lengths of entangled bundles, preferentially remove metal impurities, and introduce functional groups on the tube sidewalls (Shen et al. 2005). Because physicochemistry can potentially influence biological fate and transport and resultant health effects, it is of interest to understand how manipulation (i.e., purification and grinding) of SW-CNTs in our study influences these characteristics. Raman spectroscopy has been used as a means to not only characterize the surface chemistry and carbon bond defects of carbon-based nanomaterials but also evaluate the diameter, length, chirality, and matrix effects of SW-CNTs and MW-CNTs (Saito and Kataura 2001; Shen et al. 2005). The intensity of the G band in Raman spectroscopy represents the in-plane stretching vibration of the carbon–carbon bonds within the graphene sheets. The G band is commonly composed of two separate peaks: higher frequency peak (G2) due to vibrations along the axis and one of lower frequency (G1) caused by vibrations along the tube circumference (Shen et al. 2005). The patterns of the G1 and G2 bands have been reported to shift depending on the presence of semiconducting versus metallic tubes (Brown et al. 2001; Shen et al. 2005). Comparing the G band spectrum of our FeSW-CNT versus cSW-CNT illustrates a shift of G2 to a lower frequency for cSW-CNTs (Figure 7), which is consistent with prior studies showing that nitric acid treatment preferentially eliminates metallic and smaller diameter tubes (Strano et al. 2003; Shen et al. 2005).

The D band is useful in characterizing the carbon bond defect density of SW-CNT samples. The D band involves the resonantly enhanced scattering of an electron via photon emission by a defect that breaks the symmetry of the graphene plane (Strano et al. 2003). The addition of functional groups and defects into the tube wall typically causes an upshift of the D band frequency, as well as an increase in the D bandwidth (Shen et al. 2005). Studies comparing the effects of grinding and functionalization on the Raman spectral pattern of CNTs have shown a shift in the D and G band intensity and line shape. The physical grinding of MW-CNTs causes an increase in the D and G band intensity ratio observed with Raman spectroscopy, whereas heating these materials to high temperatures (2400°C) reanneals the carbon bond defects, restores the G band intensity, and lowers the D to G band intensity ratio (Fenoglio et al. 2008). Increasing functionalization (e.g., increasing functional groups per 1000 carbon atoms) of SW-CNTs has shown to sharply increase the height of the D band, which appears to be preferential to metallic nanotubes (Strano et al. 2003).

Although there appeared to be a change in the G band line shape, the relative intensity of the D band of cSW-CNTs decreased compared with FeSW-CNTs, suggesting that structural defects or functional groups were not introduced in the purification and aerosolization employed in this study. It has been suggested that Raman spectroscopy is insensitive to detecting low degrees of sidewall damage and scanning tunneling microscopy is better suited for quantifying the degree of structural integrity (Wang et al. 2007). Despite this, our Raman findings suggest that the purification process employed in our study removes amorphous carbon and/or nanotubes exhibiting disordered graphitic bonds (as observed with the decrease in the relative D band intensity) and also removes metallic SW-CNTs (as characteristic of G band pattern shifts). Further, it appears as though the aerosolization system (i.e., mechanical forces of the grinding wheel) does not introduce carbon defects significant enough to be detected by Raman spectroscopy. Therefore, the aerosolization system designed in this study would be useful and appropriate for comparing the effects of different physicochemical characteristics of SW-CNTs in future toxicological inhalation studies without confounding these results with chemical or structural changes associated with the method of administration.

In summary, the aerosolization system developed in this study allows for delivery of carbon-based nanomaterials (including FeSW-CNTs, cSW-CNTs, and ultrafine carbon black), representing different physical, chemical, and morphological properties but similar aerosol characteristics, from a dry bulk medium into respirable airborne particles for administration into a nose-only inhalation system. Future research utilizing this system will offer the opportunity for a systematic approach in evaluating the relationship between particle physicochemistry and toxicity by exposing animals to aerosolized carbon-based nanomaterials of different chemistry and morphology in a manner that is physiologically and environmentally relevant. This system should also prove useful for testing of small quantities of new nanomaterials as they are being produced in research and development to better understand their relative biocompatibility or toxicity compared with other particles for which the hazards are better established. As the database of hazard information develops for different nanomaterials, relating airborne particle characteristics in experimental studies to those in human exposure settings will be critical for establishing exposure/dose-response relationships and standards to protect human health.

REFERENCES

Alivisatos, P. (2000). Colloidal Quantum Dots from Scaling Laws to Biological Applications. *Pure Appl. Chem.*, 72(1–2):3–9.

Baron, P. A., Deye, G. J., Chen, B. T., Schwegler-Berry, D. E., Shvedova, A. A., and Castranova, V. (2008). Aerosolization of Single-Walled Carbon Nanotubes for an Inhalation Study. *Inhal. Toxicol.*, 20(8):751–760.

Baughman, R. H. (2000). Materials Science: Putting a New Spin on Carbon Nanotubes. *Science*, 290(5495):1310–1311.

Bianco, A., Hoebeke, J., Kostarelos, K., Prato, M., and Partidos, C. D. (2005a). Carbon Nanotubes: On the Road to Deliver. *Curr. Drug Deliv.*, 2(3):253–259.

Bianco, A., Kostarelos, K., Partidos, C. D., and Prato, M. (2005b). Biomedical Applications of Functionalised Carbon Nanotubes. *Chem. Commun. (Camb)*, 5:571–577.

Bianco, A., Kostarelos, K., and Prato, M. (2005c). Applications of Carbon Nanotubes in Drug Delivery. *Curr. Opin. Chem. Biol.*, 9(6):674–679.

Bianco, A., and Prato, M. (2003). Can Carbon Nanotubes be Considered Useful Tools for Biological Applications? *Adv. Mater.*, 15:1765–1768.

Bottini, M., Bruckner, S., Nika, K., Bottini, N., Bellucci, S., Magrini, A., Bergamaschi, A., and Mustelin, T. (2006). Multi-Walled Carbon Nanotubes Induce T Lymphocyte Apoptosis. *Toxicol. Lett.*, 160(2):121–126.

British Standards Institution. (1993). *Workplace Atmospheres—Size Fraction Definitions for Measurement of Airborne Particles* (Vol. BS EN 481:1993). British Standards Institution (BSI) in cooperation with the European Committee for Standardization (CEN), London.

Brown, S. D. M., Jorio, A., Corio, P., Dresselhaus, M. S., Dresselhaus, G., Saito, R., and Kneipp, K. (2001). Origin of the Breit-Wigner-Fano Lineshape of the Tangential G-Band Feature of Metallic Carbon Nanotubes. *Phys. Rev. B*, 63:1554141–1554148.

Chen, X., Lee, G. S., Zettl, A., and Bertozzi, C. R. (2004). Biomimetic Engineering of Carbon Nanotubes by Using Cell Surface Mucin Mimics. *Angew Chem. Int. Ed. Engl.*, 43(45):6111–6116.

Cui, D. (2005). Effect of Single Wall Carbon Nanotubes on Human HEK293 Cells. *Toxicol. Lett.*, 155:73–85.

Dames, P., Gleich, B., Flemmer, A., Hajek, K., Seidl, N., Wiekhorst, F., Eberbeck, D., Bittmann, I., Bergemann, C., Weyh, T., Trahms, L., Rosenecker, J., and Rudolph, C. (2007). Targeted Delivery of Magnetic Aerosol Droplets to the Lung. *Nat. Nanotechnol.*, 2(8):495–499.

Ding, L., Stilwell, J., Zhang, T., Elboudwarej, O., Jiang, H., Selegue, J. P., Cooke, P. A., Gray, J. W., and Chen, F. F. (2005). Molecular Characterization of the Cytotoxic Mechanism of Multiwall Carbon Nanotubes and Nano-Onions on Human Skin Fibroblast. *Nano Lett.*, 5(12):2448–2464.

Drexler, K. E. (1992). *Nanosystems: Molecular, Machinery, Manufacturing, and Composition*. Wiley-Interscience Publication, New York, NY.

Dumortier, H., Lacotte, S., Pastorin, G., Marega, R., Wu, W., Bonifazi, D., Briand, J. P., Prato, M., Muller, S., and Bianco, A. (2006). Functionalized Carbon Nanotubes Are Non-Cytotoxic and Preserve the Functionality of Primary Immune Cells. *Nano Lett.*, 6(7):1522–1528.

El-Gendy, N., and Berkland, C. (2009). Combination Chemotherapeutic Dry Powder Aerosols via Controlled Nanoparticle Agglomeration. *Pharm. Res.*, 26(7):1752–1763.

Fenoglio, I., Greco, G., Tomatis, M., Muller, J., Raymundo-Pinero, E., Beguin, F., Fonseca, A., Nagy, J. B., Lison, D., and Fubini, B. (2008). Structural Defects Play a Major Role in the Acute Lung Toxicity of Multiwall Carbon Nanotubes: Physicochemical Aspects. *Chem. Res. Toxicol.*, 21(9): 1690–1697.

Foldvari, M., and Bagonluri, M. (2008a). Carbon Nanotubes as Functional Excipients for Nanomedicines: I. Pharmaceutical Properties. *Nanomedicine*, 4(3):173–182.

Foldvari, M., and Bagonluri, M. (2008b). Carbon Nanotubes as Functional Excipients for Nanomedicines: II. Drug Delivery and Biocompatibility Issues. *Nanomedicine*, 4(3):183–200.

Fortina, P., Kricka, L. J., Surrey, S., and Grodzinski, P. (2005). Nanobiotechnology: The Promise and Reality of New Approaches to Molecular Recognition. *Trends Biotechnol.*, 23(4):168–173.

Gao, M., Huang, S., Dai, L., Wallace, G., Gao, R., and Wang, Z. (2000). Aligned Coaxial Nanowires of Carbon Nanotubes Sheathed with Conducting Polymers. *Angew Chem. Int. Ed. Engl.*, 39(20):3664–3667.

Hu, H., Haddon, R. C., Ni, Y., Montana, V., and Parpura, V. (2004). Chemically Functionalized Carbon Nanotubes as Substrates for Neuronal Growth. *Nano Lett.*, 4:507–511.

Hu, J. T., Odom, T. W., and Lieber, C. M. (1999). Chemistry and Physics in One Dimension: Synthesis and Properties of Nanowires and Nanotubes. *Accounts Chem. Res.*, 32(5):435–445.

International Organization for Standardization. (1995). *Air Quality—Particle Size Fraction Definitions for Health-Related Sampling* [Vol. ISO 7708:1995(E)]. International Organization for Standardization (ISO), Geneve, Switzerland.

Jia, G., Wang, H., Yan, L., Wang, X., Pei, R., Yan, T., Zhao, Y., and Guo, X. (2005). Cytotoxicity of Carbon Nanomaterials: Single-Wall Nanotube, Multi-Wall Nanotube, and Fullerene. *Environ. Sci. Technol.*, 39(5):1378–1383.

Katz, E., and Willner, I. (2004). Biomolecule-Functionalized Carbon Nanotubes: Applications in Nanobioelectronics. *Chemphyschem.*, 5(8): 1084–1104.

Ku, B., Maynard, A. D., Baron, P. A., and Deye, G. J. (2007). Observation and Measurement of Anomalous Responses in a Differential Mobility Analyzer Caused by Ultrafine Fibrous Carbon Aerosols. *J. Electrostat.*, 65:542–548.

Lam, C. W., James, J. T., McCluskey, R., and Hunter, R. L. (2004). Pulmonary Toxicity of Single-Wall Carbon Nanotubes in Mice 7 and 90 Days After Intratracheal Instillation. *Toxicol. Sci.*, 77(1):126–134.

Li, J. G., Li, W. X., Xu, J. Y., Cai, X. Q., Liu, R. L., Li, Y. J., Zhao, Q. F., and Li, Q. N. (2007). Comparative Study of Pathological Lesions Induced by Multiwalled Carbon Nanotubes in Lungs of Mice by Intratracheal Instillation and Inhalation. *Environ. Toxicol.*, 22(4):415–421.

Lieber, C. (2003). Nanoscale Science and Technology: Building a Big Future from Small Things. *MRS Bull.*, 28(77):486–491.

Lovat, V., Pantarotto, D., Lagostena, L., Cacciari, B., Grandolfo, M., Righi, M., Spalluto, G., Prato, M., and Ballerini, L. (2005). Carbon Nanotube Substrates Boost Neuronal Electrical Signaling. *Nano Lett.*, 5(6):1107–1110.

Magrez, A., Kasas, S., Salicio, V., Pasquier, N., Seo, J. W., Celio, M., Catsicas, S., Schwaller, B., and Forro, L. (2006). Cellular Toxicity of Carbon-Based Nanomaterials. *Nano Lett.*, 6(6):1121–1125.

Ma-Hock, L., Burkhardt, S., Strauss, V., Gamer, A. O., Wiench, K., van Ravenzwaay, B., and Landsiedel, R. (2009). Development of a Short-Term Inhalation Test in the Rat Using Nano-Titanium Dioxide as a Model Substance. *Inhal. Toxicol.*, 21(2):102–118.

Manna, S. K., Sarkar, S., Barr, J., Wise, K., Barrera, E. V., Jejelowo, O., Rice-Ficht, A. C., and Ramesh, G. T. (2005). Single-Walled Carbon Nanotube Induces Oxidative Stress and Activates Nuclear Transcription Factor-KappaB in Human Keratinocytes. *Nano Lett.*, 5(9):1676–1684.

Martin, A. R., Thompson, R. B., and Finlay, W. H. (2008). MRI Measurement of Regional Lung Deposition in Mice Exposed Nose-Only to Nebulized Superparamagnetic Iron Oxide Nanoparticles. *J. Aerosol Med. Pulm. Drug Deliv.*, 21(4):335–342.

Mattson, M. P., Haddon, R. C., and Rao, A. M. (2000). Molecular Functionalization of Carbon Nanotubes and Use as Substrates for Neuronal Growth. *J. Mol. Neurosci.*, 14(3):175–182.

Mitchell, L. A., Gao, J., Wal, R. V., Gigliotti, A., Burchiel, S. W., and McDonald, J. D. (2007). Pulmonary and Systemic Immune Response to Inhaled Multiwalled Carbon Nanotubes. *Toxicol. Sci.*, 100(1):203–214.

Monteiro-Riviere, N. A., Nemanich, R. J., Inman, A. O., Wang, Y. Y., and Riviere, J. E. (2005). Multi-Walled Carbon Nanotube Interactions with Human Epidermal Keratinocytes. *Toxicol. Lett.*, 155(3):377–384.

Muller, J., Huaux, F., Fonseca, A., Nagy, J. B., Moreau, N., Delos, M., Raymundo-Pinero, E., Beguin, F., Kirsch-Volders, M., Fenoglio, I., Fubini, B., and Lison, D. (2008). Structural Defects Play a Major Role in the Acute Lung Toxicity of Multiwall Carbon Nanotubes: Toxicological Aspects. *Chem. Res. Toxicol.*, 21(9):1698–1705.

Muller, J., Huaux, F., Moreau, N., Misson, P., Heilier, J. F., Delos, M., Arras, M., Fonseca, A., Nagy, J. B., and Lison, D. (2005). Respiratory Toxicity of Multi-Wall Carbon Nanotubes. *Toxicol. Appl. Pharmacol.*, 207(3):221–231.

Navrotsky, A. (2001). Thermochemistry of Nanomaterials. *Nanoparticles Environ.*, 44:73–103.

Ostraat, M. L., Swain, K. A., and Krajewski, J. J. (2008). SiO_2 Aerosol Nanoparticle Reactor for Occupational Health and Safety Studies. *J. Occup. Environ. Hyg.*, 5(6):390–398.

Park, E. J., Brasuel, M., Behrend, C., Philbert, M. A., and Kopelman, R. (2003a). Ratiometric Optical PEBBLE Nanosensors for Real-Time Magnesium Ion Concentrations Inside Viable Cells. *Anal. Chem.*, 75(15):3784–3791.

Park, K. H., Chhowalla, M., Iqbal, Z., and Sesti, F. (2003b). Single-Walled Carbon Nanotubes Are a New Class of Ion Channel Blockers. *J. Biol. Chem.*, 278(50):50212–50216.

Poland, C. A., Duffin, R., Kinloch, I., Maynard, A., Wallace, W. A., Seaton, A., Stone, V., Brown, S., Macnee, W., and Donaldson, K. (2008). Carbon Nanotubes Introduced into the Abdominal Cavity of Mice Show Asbestos-Like Pathogenicity in a Pilot Study. *Nat. Nanotechnol.*, 3(7):423–428.

Ryman-Rasmussen, J. P., Tewksbury, E. W., Moss, O. R., Cesta, M. F., Wong, B. A., and Bonner, J. C. (2008). Inhaled Multi-Walled Carbon Nanotubes Potentiate Airway Fibrosis in Murine Allergic Asthma. *Am. J. Respir. Cell Mol. Biol.*, 40(3):349–358.

Saito, N., and Kataura, H. (2001). Optical Properties and Raman Spectroscopy of Carbon Nanotubes, in *Carbon Nanotubes*, M. S. Dresselhaus, G. Dresselhaus, and P. Avouris, eds., Springer-Verlag Berlin, Berlin, pp. 213–246.

Sayes, C. M., Marchione, A. A., Reed, K. L., and Warheit, D. B. (2007). Comparative Pulmonary Toxicity Assessments of C60 Water Suspensions in Rats: Few Differences in Fullerene Toxicity In Vivo in Contrast to In Vitro Profiles. *Nano Lett.*, 7(8):2399–2406.

Schipper, M. L., Nakayama-Ratchford, N., Davis, C. R., Kam, N. W., Chu, P., Liu, Z., Sun, X., Dai, H., and Gambhir, S. S. (2008). A Pilot Toxicology Study of Single-Walled Carbon Nanotubes in a Small Sample of Mice. *Nat. Nanotechnol.*, 3(4):216–221.

Schmoll, L. H., Elzey, S., Grassian, V. H., and O'Shaughnessy, P. T. (2009). Nanoparticle Aerosol Generation Methods from Bulk Powders for Inhalation Exposure Studies. *Nanotoxicol.*, 3(4):265–275.

Shen, K., Curran, S., Xu, H., Rogelj, S., Jiang, Y., Dewald, J., and Pietrass, T. (2005). Single-Walled Carbon Nanotube Purification, Pelletization, and Surfactant-Assisted Dispersion: A Combined TEM and Resonant Micro-Raman Spectroscopy Study. *J. Phys. Chem. B*, 109:4455–4463.

Shvedova, A. A., Kisin, E., Murray, A. R., Johnson, V. J., Gorelik, O., Arepalli, S., Hubbs, A. F., Mercer, R. R., Keohavong, P., Sussman, N., Jin, J., Yin, J., Stone, S., Chen, B. T., Deye, G., Maynard, A., Castranova, V., Baron, P. A., and Kagan, V. E. (2008). Inhalation vs. Aspiration of Single-Walled Carbon Nanotubes in C57BL/6 Mice: Inflammation, Fibrosis, Oxidative Stress, and Mutagenesis. *Am. J. Physiol. Lung Cell. Mol. Physiol.*, 295(4):L552–L565.

Singh, R., Pantarotto, D., Lacerda, L., Pastorin, G., Klumpp, C., Prato, M., Bianco, A., and Kostarelos, K. (2006). Tissue Biodistribution and Blood Clearance Rates of Intravenously Administered Carbon Nanotube Radiotracers. *Proc. Natl. Acad. Sci. USA*, 103(9):3357–3362.

Smalley, R. (2001). Wires of Wonder. *Technol. Rev.*, 104(2):86–91.

Strano, M. S., Dyke, C. A., Usrey, M. L., Barone, P. W., Allen, M. J., Hongwei Shan, H., Kittrell, C., Hauge, R. H., Tour, J. M., and Smalley, R. E. (2003). Electronic Structure Control of Single-Walled Carbon Nanotube Functionalization. *Science*, 301:1519–1522.

Sung, J. C., Padilla, D. J., Garcia-Contreras, L., Verberkmoes, J. L., Durbin, D., Peloquin, C. A., Elbert, K. J., Hickey, A. J., and Edwards, D. A. (2009). Formulation and Pharmacokinetics of Self-Assembled Rifampicin Nanoparticle Systems for Pulmonary Delivery. *Pharm. Res.*, 26(8):1847–1855.

Teague, S. V., Veranth, J. M., Aust, A. E., and Pinkerton, K. E. (2005). Dust Generator for Inhalation Studies with Limited Amounts of Archived Particulate Matter. *Aerosol Sci. Technol.*, 39:85–91.

Tian, F., Cui, D., Schwarz, H., Estrada, G. G., and Kobayashi, H. (2006). Cytotoxicity of Single-Wall Carbon Nanotubes on Human Fibroblasts. *Toxicol. In Vitro*, 20(7):1202–1212.

Tong, H., McGee, J. K., Saxena, R. K., Kodavanti, U. P., Devlin, R. B., and Gilmour, M. I. (2009). Influence of Acid Functionalization on the Cardiopulmonary Toxicity of Carbon Nanotubes and Carbon Black Particles in Mice. *Toxicol. Appl. Pharmacol.*, 239(3):224–232.

US Environmental Protection Agency. (1999). *Compendium of Methods for the Determination of Inorganic Compounds in Ambient Air. Compendium Method IO-3.4. Determination of Metals in Ambient Particulate Matter Using Inductively Coupled Plasma (ICP) Spectroscopy.* Center for Environmental Research Information, Office of Research and Development, US Environmental Protection Agency (US EPA), Cincinnati, OH.

Usui, Y., Aoki, K., Narita, N., Murakami, N., Nakamura, I., Nakamura, K., Ishigaki, N., Yamazaki, H., Horiuchi, H., Kato, H., Taruta, S., Kim, Y. A., Endo, M., and Saito, N. (2008). Carbon Nanotubes with High Bone-Tissue Compatibility and Bone-Formation Acceleration Effects. *Small*, 4(2):240–246.

Wang, Y., Shan, H., Hauge, R. H., Pasquali, M., and Smalley, R. E. (2007). A Highly Selective, One-Pot Purification Method for Single-Walled Carbon Nanotubes. *J. Phys. Chem. B*, 111(6):1249–1252.

West, J. L., and Halas, N. J. (2003). Engineered Nanomaterials for Biophotonics Applications: Improving Sensing, Imaging, and Therapeutics. *Ann. Rev. Biomed. Eng.*, 5:285–292.

Yang, G.-S., Teague, S., Pinkerton, K., and Kennedy, I. M. (2001). Synthesis of an Ultrafine Iron and Soot Aerosol for the Evaluation of Particle Toxicity. *Aerosol Sci. Technol.*, 35:759–766.

Zavaleta, C., de la Zerda, A., Liu, Z., Keren, S., Cheng, Z., Schipper, M., Chen, X., Dai, H., and Gambhir, S. S. (2008). Noninvasive Raman Spectroscopy in Living Mice for Evaluation of Tumor Targeting with Carbon Nanotubes. *Nano Lett.*, 8(9):2800–2805.